Proceedings of the 1st Global Power and Propulsion Forum
GPPF 2017
Jan 16-18, 2017, Zurich, Switzerland
www.pps.global

GPPF-2017-9

ESTIMATION OF THE HEAD LOSS IN THE ANNULAR CHAMBER OF MULTISTAGE CENTRIFUGAL PUMPS FEATURING A COMPACT DESIGN

Federico Fontana
University of Padua
Federico.fontana.3@phd.unipd.it
Padua, Italy

ABSTRACT

Radial flow, multistage centrifugal pumps made by sheet metal forming usually feature a compact design. In these machines the abrupt diffusion of the flow and the reversal of its direction cause a head loss across the annular chamber which connects the impeller with the return channels. In this paper a corresponding loss coefficient was defined as the ratio between the total head loss and the dynamic head at the impeller outlet. Numerical estimations of such loss coefficient are reported for several stage designs and operating conditions. These data may support both the design and the performance analysis of multistage, compact design pumps. A physical interpretation of the phenomenology is suggested.

INTRODUCTION

Compact Design (CD) is a common solution among mass production, Radial flow Multistage Pumps (RMPs), for submersible and surface applications, featuring vertical or horizontal axis. In this solution, the impeller flow is collected into an annular chamber that leads to the return channels. The latter guide the flow either to the next stage or to the pump delivery while reducing the tangential velocity, ideally to zero. The compact design requires to solve some specific issues not present in traditional multistage pumps that do not feature annular chambers. The CD of RMPs has gained popularity only recently and the related guidelines are still limited. Moreover, the relevant literature focuses only on the geometry of either the impeller or the return channels.

In particular, Pedersen et al [1] and Byskov et al [2] studied the unsteady flow in the impeller of a CD-RMP by experiments (PIV and LDV measurements) and LES-CFD, respectively. Wang et al [3] optimized the impeller geometry of a deep well pump by applying a regression technique to a set of CFD simulations. Zhou et al [4] analysed, both numerically and experimentally, the influence of the diameter of the impeller driving disk on performance, efficiency and axial thrust of a CD pump. In [5], the authors investigated the effects of the blade number and the splitter blade length on performance and efficiency of a submersible pump.

In turn, other works focused on the return channels for CD stages. For example, Zhou et al [6] used CFD models and experiments to develop and investigate the return channels of a submersible, borehole pump. Zhang et al [7] proposed a modification of the design strategy presented in [6]. A similar design method for the return channels was developed at University of Kaiserslautern (see for instance [8]). For such design, the unsteady fluid dynamic behaviour was studied by means of CFD in [9]. All the previous design methods result in return channels with a complex 3D shapes. Accordingly, moulding or casting are the best suited manufacturing technologies for mass production of these shapes.

On the other hand, sheet metal forming and welding is becoming a leading technology for CD-RPMs [3]. More details about this type of machines are provided in [10]. This technology is very advantageous when 2D profiles (i.e. cylindrical blades) are adopted for both the impeller blades and the walls of the return channels. In fact, this solution allows to use very competitive and robust welding processes, that in turn impact significantly the manufacturing cost. As a consequence, the 3D designs considered in the previous references are not suitable for these machines.

When the return channels are obtained from cylindrical blades, regardless of the manufacturing technology, a significant head loss is expected in the annular chamber, due to the abrupt diffusion of the flow. This issue is very specific of the CD pump type and, to the author's knowledge, it is not discussed in the literature. In the light of this, the present paper investigates numerically the head loss between the impeller outlet and the return channel inlet. In particular, five different stages of CD-RMPs made by sheet metal forming were analysed. The study aims at identifying the parameter that mostly affect such loss, explaining the basic flow mechanism, and providing a correlation for the design and the performance analysis of the CD-RMPs.

METHODOLOGY

The sketch in Fig. 1 shows the main geometrical features and the corresponding parameters of a generic CD stage. The

flow path through the stage is also shown schematically in the figure, by means of arrows. With reference to a meridional section plane, the main flow enters the impeller axially and leaves it with a dominating radial velocity and weaker axial component directed toward the return channels. In the annular chamber, the flow turns its radial direction from outward to inward, and meanwhile it approaches the return channel inlet. In the return channels the flow moves radially inward and its tangential velocity is reduced ideally to zero.

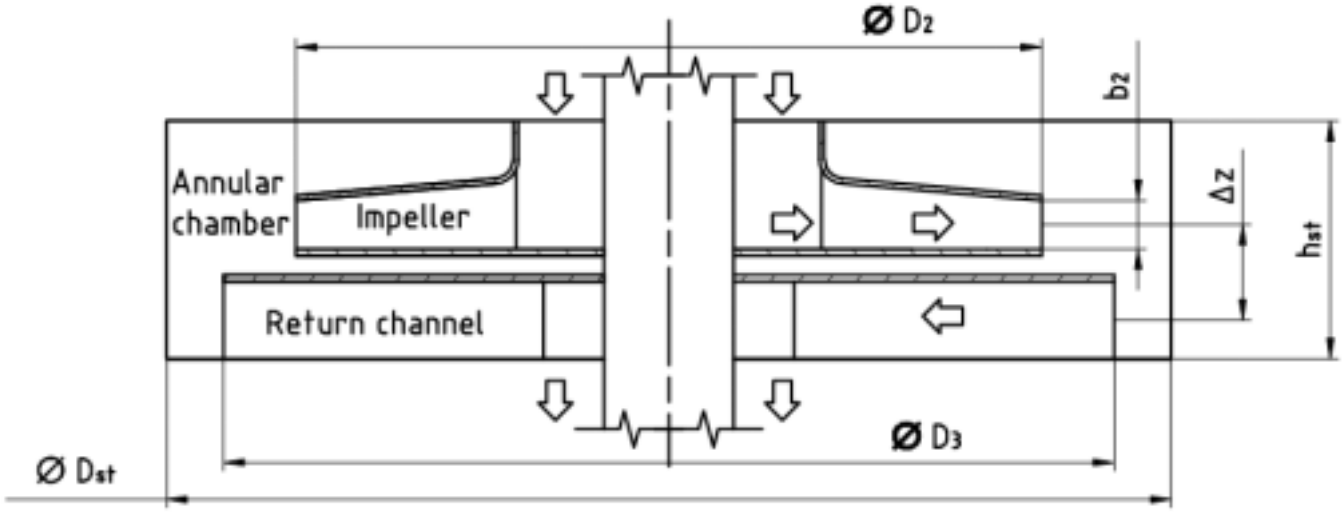

Fig. 1: schematic representation of a meridional section of a generic stage. The impeller, one return channel and the annular chamber are indicated. The flow path of the main stream is represented by arrows. The main geometrical features of the stage are referenced.

In the present study, five stages belonging to industrial RMPs were considered. This choice was due: (i) to the rather strict constraints found in the mass production of this type of pumps, which makes it preferable to consider only stages from real industrial pumps, and (ii) to the availability of experimental data for the validation of the numerical models. The stages differ one each other in the geometry of the impeller and of the return channels and in the maximum diameter of the stage. Table 1 associates each case study (i.e., each stage geometry) with an alpha-numeric code and presents the main geometrical parameters as dimensionless ratios (refer also to Fig. 1).

Case study	D_3/D_2	D_{st}/D_2	$\Delta z/D_2$	h_{st}/D_2	b_2/h_{st}
C1	1.24	1.40	0.086	0.26	0.10
C3	1.24	1.40	0.121	0.26	0.17
C4	1.20	1.35	0.096	0.18	0.12
C6	1.24	1.40	0.135	0.31	0.19
C9	1.19	1.35	0.129	0.32	0.20

Table 1. Case studies and corresponding dimensionless values of the main geometrical features.

For each case study, a minimum of six duty points centred on the best efficiency point (BEP) was investigated for a rotational speed of 2900 rpm. The Reynolds number defined according to the velocity at the impeller blade tip and the blade tip radius (Re_T) ranges between 460'000 and 640'000. Therefore, the flow regime is fully turbulent for all cases and the influence of Re_T on the results is neglected in the following.

Geometrical parameters considered in the study

In the analysis of the data, the following geometrical features were considered:

- Geometrical expansion ratio (GER): it is the ratio between the impeller blade height and the stage height (b_2 and h_{st} in Fig. 1, respectively). This ratio represents the sudden enlargement of the through-flow section in a meridional plane.
- Relative axial distance (RAD): it is the ratio of the axial distance between the impeller and the return channels (Δz in Fig. 1) to the impeller outer diameter, D_2. This quantity represents both the curvature of the idealized flow path in a meridional plane and the length of the path from the impeller to the return channels. In fact, with reference to a meridional plane, the flow path from the impeller outlet to the return channel inlet can ideally be represented as half of an ellipse, having the semi-axes equal to:

$$a = \frac{Dst - D_3}{2}$$

and

$$b = \frac{\Delta z}{2},$$

respectively (see Figure 2). For all the cases considered in this study, *b* is the minor axis and it consequently determines the major curvature. Therefore, the effect of the axis *a* on the curvature is considered negligible. In turn, with reference to the 3D flow, the trajectory of a particle of fluid moving from the impeller outlet to the return channel inlet resembles an arc

of a cylindrical helix. Accordingly, its length is influenced significantly by the distance Δz.

Data Processing

The static pressure (p), total pressure ($p°$), and velocity (c) were probed on two cylindrical control surfaces located at the impeller outlet (section 2 - placed at the blade trailing edge) and at the return channel entrance (section 3 - placed at the blade leading edge), respectively.

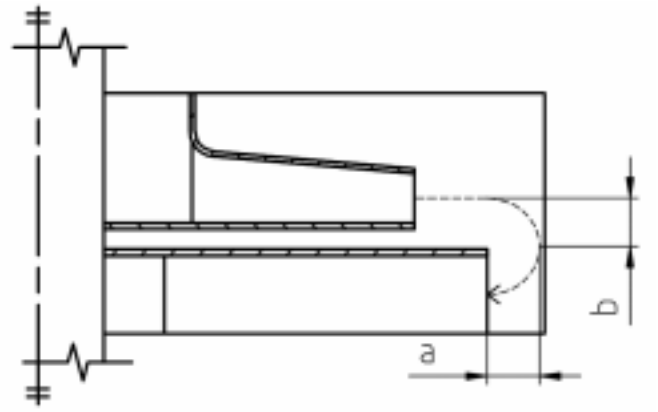

Fig. 2: ideal representation of the meridional flow path in the annular chamber by means of a semi-ellipse, which axes are quoted in the figure.

These data were used to estimate the total head loss occurring between the impeller outlet and the return channel inlet. The corresponding loss coefficient ζ was calculated as:

$$\zeta = \frac{\overline{p_2^o} - \overline{p_3^o}}{\overline{p_2^o} - \overline{p_2}}, \quad (1)$$

where over-bars indicate averaging according to the local value of the radial component of the velocity. Since the probing was performed on regular grids of equally spaced points, this averaging approximates the mass flow averaging.

Numerical model

The MRF approach was used and steady state simulations were performed. The 3D domain included one impeller channel, one return channel and the corresponding slice of the annular chamber (Fig. 3). Turbulence was simulated by means of the k-Epsilon model, with standard wall functions at the walls (y^+ ranged between 25 and 150). Almost fully structured meshes were used, with cell amounts ranging between 250k and 500k per one impeller channel and one return channel. For all meshes the maximum skewness was below 2.4 out of 4.0 and the number of severely non-orthogonal faces was below 4% of the total number of faces. The leakage flows at the impeller and at the return channels (see [8]) were neglected. The numerical model was implemented within the OpenFoam 2.1.1 environment. The complete description of the model is reported in [10].

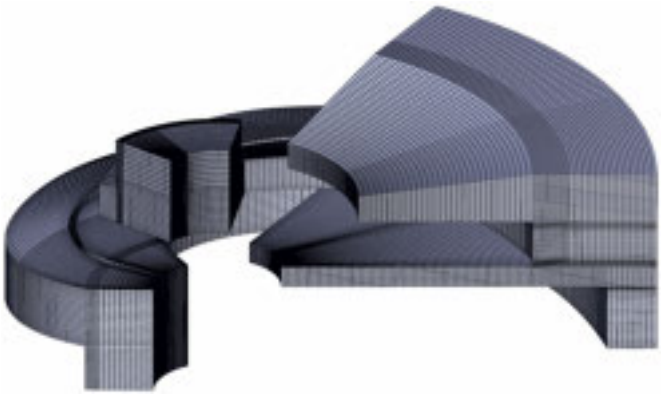

Fig. 3: mesh of the computational domain (case C6), including one impeller channel, one return channel and the corresponding slice of the annular chamber.

The same reference describes the results of the study on grid sensitivity for case C6. Accordingly, the deviation from the values of the head and torque computer for the finest mesh resolution (above 800k per flow passage) are below 1% for 200k cells and below 0.25% for 500k cells (see Fig. 4). Moreover, [10] reports the validation of the model against experimental data (see Fig. 5). In particular, the errors in the predictions of the performance and the power were equal to 5% within the nominal range of operation of the multistage pump. Both the head and the efficiency were over-estimated. These results are comparable with those of the best studies reported in the literature for multistage machines.

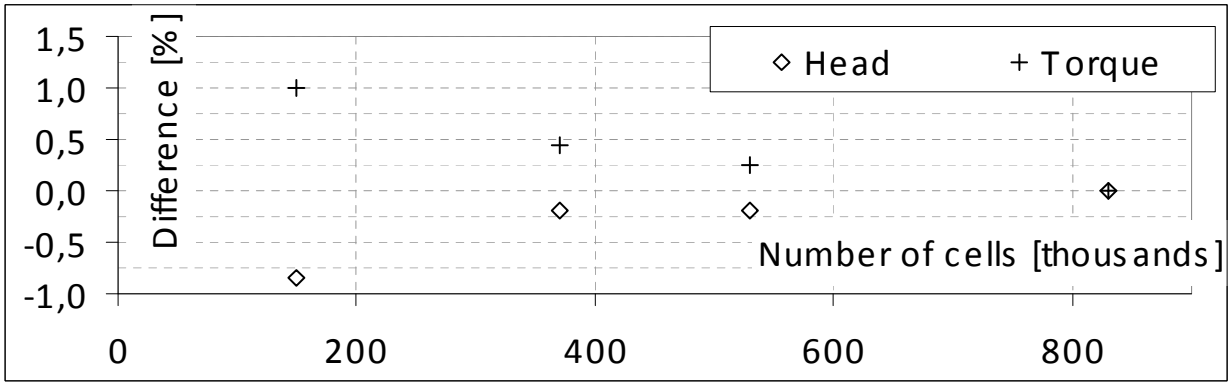

Fig. 4: results of the grid dependence investigation. The relative difference in computed head and torque with reference to the simulation of the finest mesh resolution are plotted versus the mesh size, in thousands of cells [10].

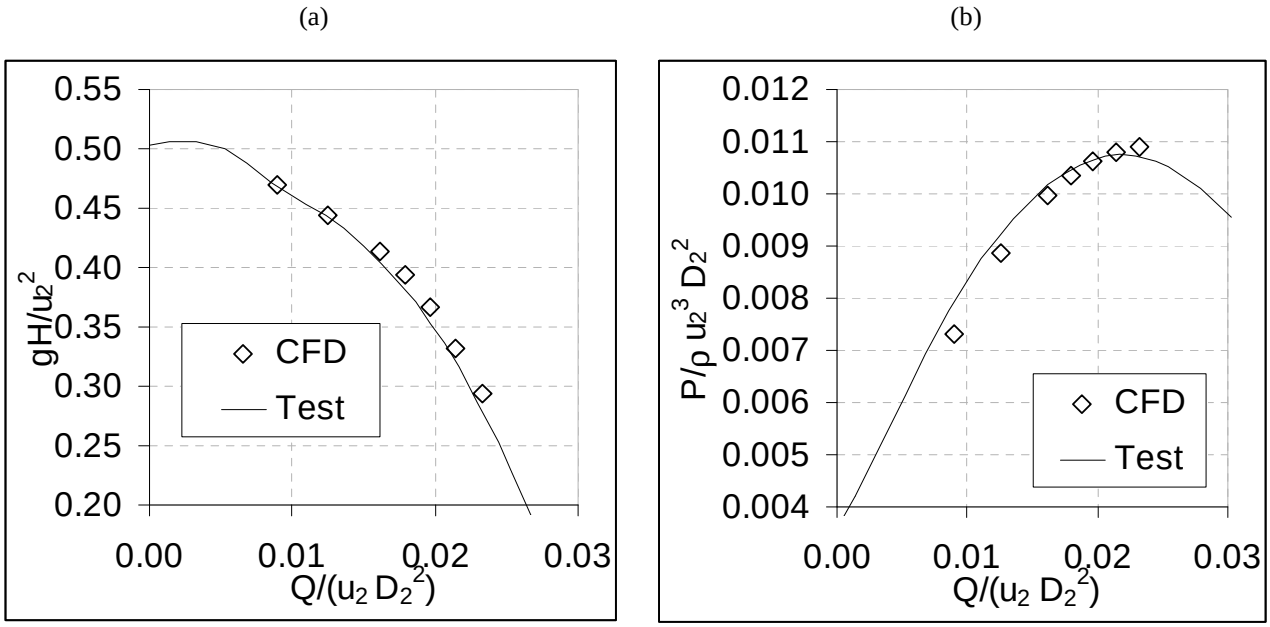

Fig. 5: comparison between measurements (solid lines) and numerical results (empty markers): a) head per stage versus the flow rate, b) absorbed power per stage versus the flow rate. All quantities are presented in dimensionless form.

The validation was performed in terms of the global parameters of the machine, namely flow rate-head, flow rate-absorbed power and flow rate-efficiency curves. In the present paper it is assumed that the agreement between the numerical and the experimental values of the global parameters provides a sufficient validation of the internal fluid dynamics (i.e. the velocity and pressure fields in the stage).

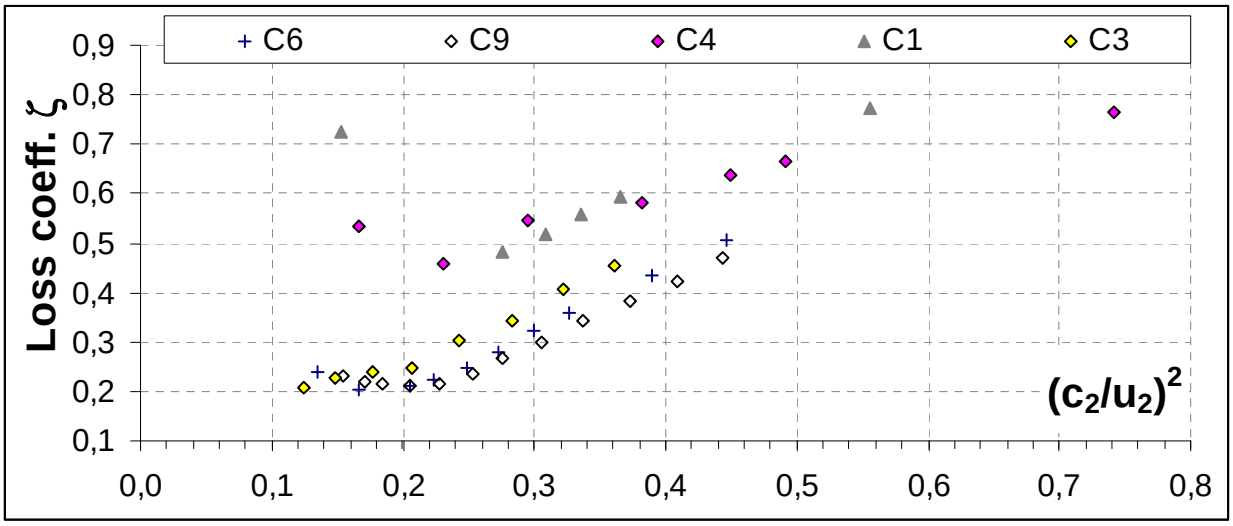

Fig. 6: loss coefficient versus the dynamic head, made dimensionless according to the dynamic head corresponding to the blade tip velocity.

RESULTS AND DISCUSSION

Fig. 6 shows ζ as a function of the flow-averaged value of the dynamic head at section 2, made dimensionless by means of the dynamic head corresponding to the blade tip velocity. The figure clearly shows a strong dependence of the loss coefficient on the dynamic head at impeller outlet for all the five cases considered.

The loss coefficient of all the series exhibits an almost linear behaviour when the dynamic head exceeds a threshold value. On the other hand, the trends below this threshold value are not univocal. In particular, series C6 and C9 show a moderate growth of ζ for the lowest values of dynamic pressure, whereas series C1 and C4 demonstrate a marked increase with decreasing dynamic pressure. Finally, series C3 exhibits a plateau close to the minima of the former series, followed by a slight decrease.

It is worth noting that the loss coefficient figures of the five series collect rather distinctly into two groups: series C1 and C4 at the top of the graph, and series C3, C6 and C9 at the bottom. The first group features values of ζ that are about 1.3-to-2 times higher than those of the other series. Moreover, the threshold value of these series is slightly larger.

Almost the same graph is obtained in case the loss coefficient is plotted against the squared value of the loading factor Ψ (i.e., the dimensionless dynamic head corresponding to the tangential velocity at the impeller outlet), as shown in Fig 7. This suggests that either the dynamic head or the square of the loading factor can be used as the independent variable in the graph. Consequently, the latter is considered hereinafter.

The red dotted lines in Fig. 7 bound the range of Ψ between 0.4 and 0.5. It is evident that the minimum of ζ (where existing, the plateau otherwise) falls within this region. Note that this range is close to that typical of BEP operation of radial flow machines [8].

Figures 6 and 7 prove that the geometrical features of the stages affect the loss coefficient ζ. In the following, the influence of the GER and of the RAD is analysed.

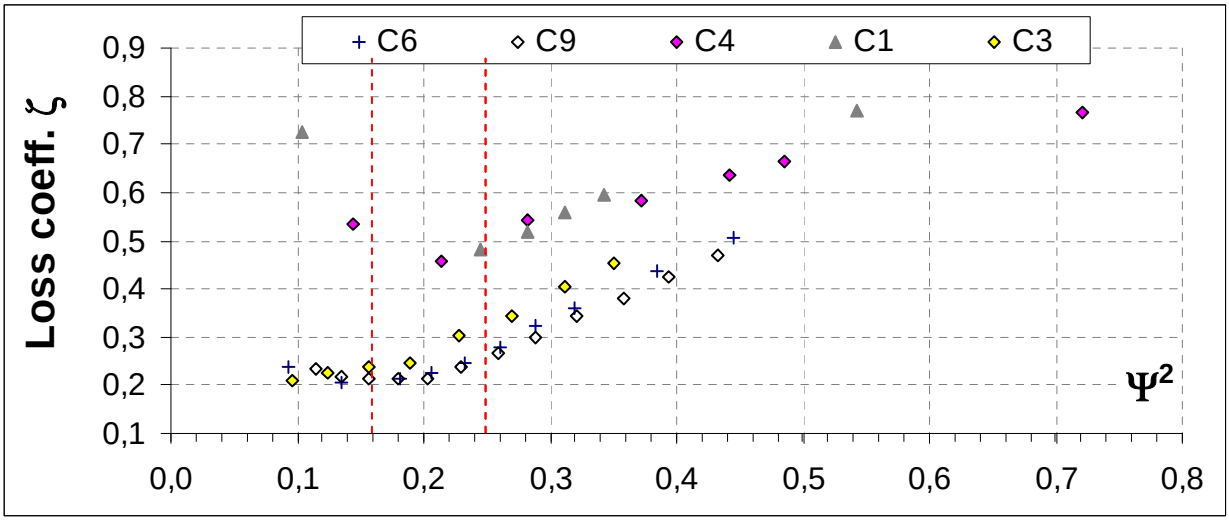

Fig. 7: loss coefficient versus the dynamic head corresponding to the tangential component of the velocity, made dimensionless according to the dynamic head corresponding to the blade tip velocity. The red dotted lines bound the range of Ψ between 0.4 and 0.5.

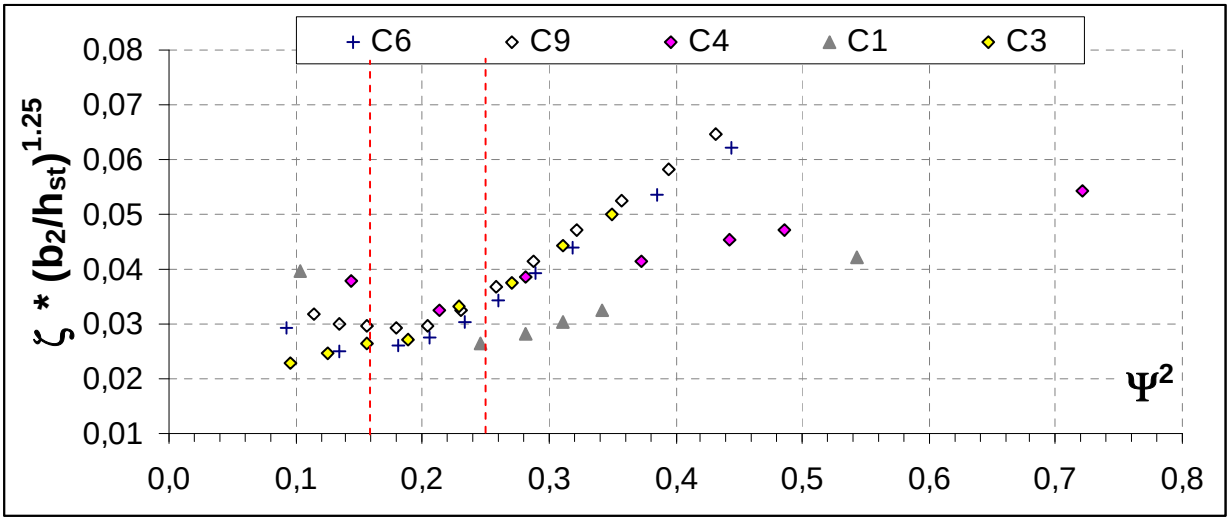

Fig. 8: product between the loss coefficient and the 1.25 power of the expansion ratio versus the dimensionless dynamic head corresponding to the tangential component of the velocity. Red dotted lines as in Fig. 7.

To account for the effect of the abrupt enlargement of the through-flow section at the impeller outlet, the product between ζ and the *k-th* power of the GER is considered. Fig. 8 was obtained by setting the value of *k* to 1.25. For this value, all series feature the minimum of ζ (the plateau for series C3) around the average value of 0.0285, within a ±12% scatter band. This result suggests that the head loss between sections 2 and 3 is mainly a diffusion loss and the expansion ratio is the geometrical parameter that mostly affects the minimum value of ζ. In fact, if one considers the ideal model of a sudden enlargement in a duct, the diffusion loss depends only on the square of the ratio between the sections upstream and downstream of the enlargement (i.e. the GER). Any other loss contribution that is superimposed can only increase the total loss, thus the diffusion loss is the minimum loss generated by the sudden enlargement. Thus, the minimum loss generated by the sudden enlargement is the diffusion loss, which magnitude is determined only by the GER. In the present case, the value

of the exponent *k* differs from 2 due to the higher complexity of the flow field in the annular chamber and to the different geometry compared with the straight duct. It is worth noting that the five series still exhibit different trends when represented according to the coordinates in figure.

The effect of the RAD is accounted by scaling the square of Ψ according to the *m-th* power of this geometrical parameter (see Fig. 9). In particular, a value of *m* equal to 0.9 moves the minimum of all series (the plateau of C3) to roughly the same value of the abscissa (about 0.025). Moreover, all series can be represented by a single correlation in the most part of the range of analysis, within a scatter band of ±15%. The edges of this band are represented in the figure by solid lines, while the average curve is shown by a broken line.

The equation corresponding to the broken line in the figure reads:

$$y = e \cdot x^3 + f \cdot x^2 + g \cdot x + h \quad (2)$$

Where the coordinates *x* and *y* are as in Fig. 9 and the coefficients are: *e* = -461.8, *f* = 69.72, *g* = -2.569 and *h* = 5.590E-2.

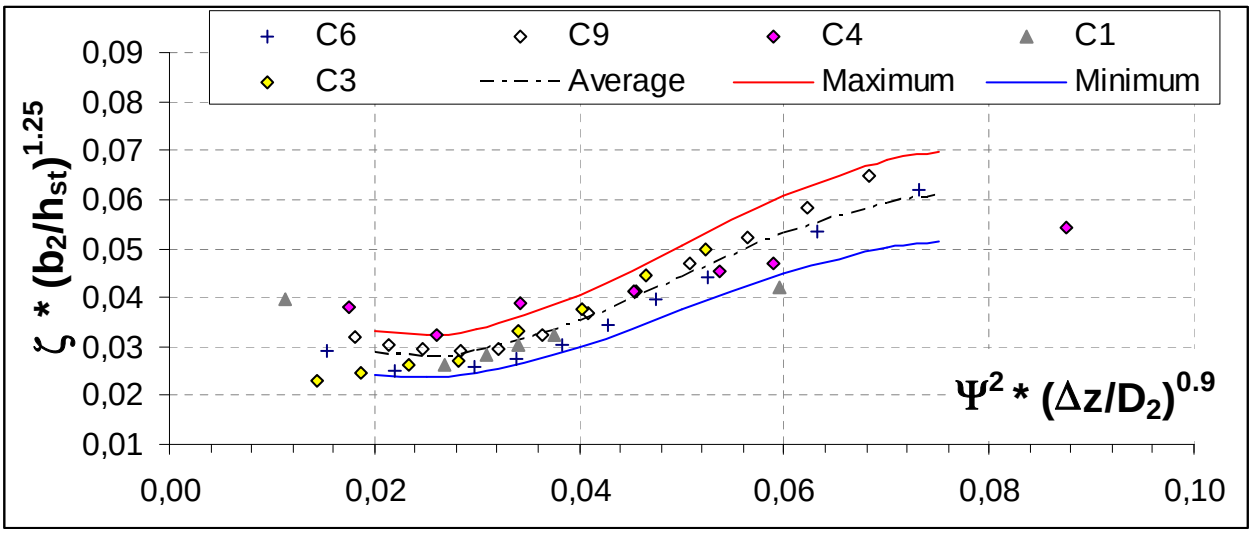

Fig. 9: product between the loss coefficient and the 1.25 power of the expansion ratio versus the product between the dimensionless dynamic head corresponding to the tangential component of the velocity and the 0.9 power of the dimensionless return channel distance.

A possible explanation for the effect of the RAD on the location of the minimum ζ is provided in the following. The location of the minimum along the abscissa is supposed to result from the sum of two loss contributions: the first one is due to the meridional curvature of the flow path; the second one to the friction loss of the main stream against either the stage casing walls or the portion of the fluid recirculating within the side volumes of the stage. The first contribution is assumed to depend on the meridional component of the velocity only (the tangential component is not subject to the meridional curvature of the flow path). In contrast, the second contribution is mainly affected by the tangential component of the velocity. In fact, the latter influences strongly both the dynamic head (that is entirely involved in the friction loss) and the length of the 3D trajectory from section 2 to section 3 (see the Methodology). As a consequence, the first contribution increases with increasing values of the meridional velocity, i.e. with decreasing tangential velocity, whereas the opposite occurs to the other.

As discussed above, larger values of the return channel distance result in a weaker meridional curvature and a longer length of the trajectory between sections 2 and 3. This reduces the loss contribution associated with the meridional component of the velocity and increases the other contribution. As a result, a larger flow rate is necessary for the first loss mechanism to prevail over the other. Accordingly, the point of minimum moves toward left in the graph, in agreement with the results in Fig. 8.

CONCLUSIONS

The head loss between the impeller outlet section and the return channel entrance were studied numerically for five different stages of multistage centrifugal pumps featuring a compact design and made by sheet metal forming. A loss coefficient was introduced to correlate the total head loss to the dynamic head at the impeller outlet.

The study highlighted that:

- the loss coefficient is a non-linear function of the dynamic head at the impeller outlet. All of the stages but one presented a minimum value of the loss coefficient, which falls roughly in the nominal range of operation.
- The loss coefficient depends on the ratio between the impeller outlet width and the stage casing height, which represents the geometrical expansion ratio of the through-flow section in the meridional plane. This parameter is the geometrical feature that exerts the most important influence on the loss coefficient, in particular on its minimum value. Accordingly, the head loss can be roughly approximated as a diffusion loss caused by the sudden enlargement.
- The axial distance between the impeller outlet and the return channel inlet determines the position of the minimum and the trend of the loss coefficient curve. A

single correlation for the five stages can be used in the nominal range of operation, provided that the effects of the expansion ratio and the return channel distance are considered.

It was found that the behaviour of the five stages is significantly different outside of the nominal range of operation. In particular, one case showed a decreasing trend of the loss coefficient with decreasing dynamic head, in contrast with the others. An explanation for this behaviour was not found. A deeper understanding of this phenomenon would be interesting from both scientific and industrial perspectives.

NOMENCLATURE

a	semi-axis of the ellipse
b	semi-axis of the ellipse
b_2	impeller outlet width
BEP	best efficiency point
c	absolute velocity of the fluid
D	diameter
g	gravitational acceleration
H	head per stage
h_{st}	stage height
P	mechanical power
p	static pressure
p°	total pressure
Q	pump flow rate
Re	Reynolds number
u	peripheral velocity of the impeller
Δz	distance between the impeller outlet section and the return channel inlet section
Ψ	loading coefficient, c_{t2}/u_2
ρ	fluid density
ζ	loss coefficient
2	(pedicle) referring to the impeller outlet section
3	(pedicle) referring to the return channel inlet section
st	(pedicle) referring to the stage casing
t	(pedicle) tangential component of the velocity
T	(pedicle) referring to the blade tip

REFERENCES

[1] Pedersen, N, Larsen, PS, and Jacobsen, CB, “Flow in a Centrifugal Pump Impeller at Design and Off-Design Conditions-Part I: Particle Image Velocimetry (PIV) and Laser Doppler Velocimetry (LDV) Measurements”, ASME J Fluids Eng, 125, 2003, pp 61-72

[2] Byskov, RK, Jacobsen, CB, and Pedersen, N, “Flow in a Centrifugal Pump Impeller at Design and Off-Design Conditions-Part II: Large Eddy Simulations”, ASME J Fluids Eng, 125, 2003, pp 73-83

[3] Wang, C, Shi, W, Zhou, L, and Lu, W, “Effect Analysis of Geometric Parameters on Stainless Steel Stamping Multistage Pump by Experimental Test and Numerical Calculation”, Advances in Mechanical Engineering, 2013, 2013, Art. ID 575731, http://dx.doi.org/10.1155/2013/575731

[4] Zhou, L, Shi, W, Li, W, and Agarval, R, “Numerical and Experimental Study of Axial Force and Hydraulic Performance in a Deep-Well Centrifugal Pump With Different Impeller Rear Shroud Radius”, ASME J Fluids Eng, 135, 2013, pp 104501-1-8

[5] Golcu, M, Pankar, Y, and Semken, Y, “Energy saving in a deep well pump with splitter blade”, Energy Conversion and Management, 47, 2006, pp 638-651

[6] Zhou, L, Shi, W, Lu, W, Hu, B, and Wu, S, “Numerical Investigations and Performance Experiments of a Deep-Well Centrifugal Pump With Different Diffusers”, ASME J Fluids Eng, 134, 2012, pp 071102-1-8

[7] Zhang, Q, Shi, W, Xu, Y, Gao, X, Wang, C, Lu, W, and Ma, D, “A New Proposed Return Guide Vane for Compact Multistage Centrifugal Pumps”, International Journal of Rotating Machinery, 2013, 2013, Art. ID 683713, http://dx.doi.org/10.1155/2013/683713

[8] Gulich, JF, “Centrifugal Pumps”, Berlin, Springer-Verlag, 2008

[9] Roclawski, H, and Hellmann, DH, “Rotor-Stator-Interaction of a Radial Centrifugal Pump Stage with Minimum Stage Diameter”, Proc. 4th WSEAS Int. Conf. on Fluid Mechanics and Aerodynamics, Elounda, Greece, 2006, pp 301-308

[10] Fontana, F, and Masi, M, “CFD modelling to aid the design of steel sheet multistage pumps”, Proc. 29th Int. Conf. on Efficiency, Cost, Optimization, Simulation and Environmental Impact of Energy Systems, Portoroz, Slovenia, 2016